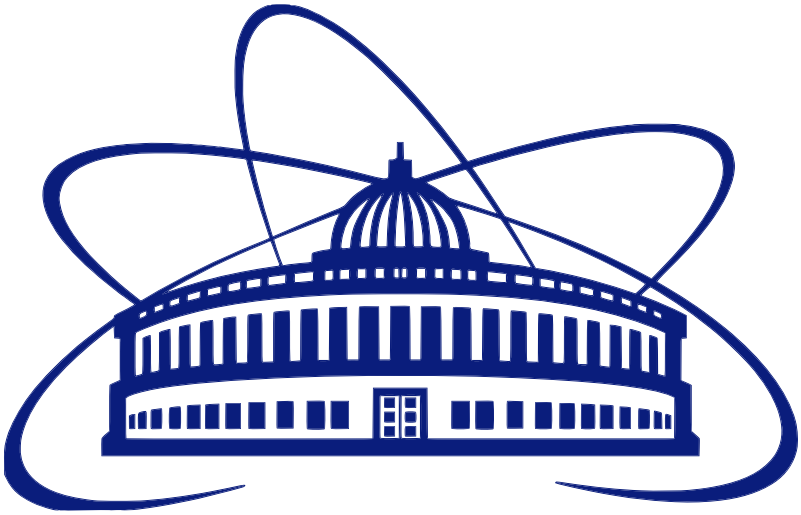

JOINT INSTITUTE FOR NUCLEAR RESEARCH

Flerov Laboratory of Nuclear Reactions

INTEREST PROGRAMME FINAL REPORT

Production and spectroscopic investigation of new neutron-rich isotopes near the neutron $N = 126$ shell closure using the multinucleon transfer reactions

Supervisor:

Dr. Viacheslav Vedeneev

FLNR, JINR

Student:

Tushar Verma, India

Indian Institute of Technology Kanpur

tusharverma218@gmail.com

Participation period:

02 March – 19 April 2026

Wave 14

Dubna, 2026

Contents

Abstract **2**

I Introduction **3**

II Theoretical Background **3**

III Experimental Setup **4**

III.A Beam and Target 4

III.B Detector Systems 5

IV Methodology **6**

V Data Analysis **6**

V.A ^{40}Ar + ^{148}Sm 6

V.B ^{40}Ar + ^{166}Er 8

V.C ^{48}Ca + ^{242}Pu 10

VI Results and Discussion **12**

VII Conclusion **14**

Acknowledgements **14**

Abstract

The study of neutron-rich heavy nuclei provides insight into nuclear structure and shell effects in regions far from stability. In this work, α-decay spectroscopy has been performed on nuclei produced in multinucleon transfer reactions: ^{40}Ar + ^{148}Sm, ^{40}Ar + ^{166}Er, and ^{48}Ca + ^{242}Pu.

Experimental data, obtained as one-dimensional energy spectra, were analyzed using Origin software. Gaussian peak fitting was applied to extract α-decay energies, and the resulting peak positions were compared with evaluated nuclear data to assign isotopes and construct decay chains. In the ^{40}Ar + ^{148}Sm reaction, mercury isotopes in the range ^{180}Hg to ^{185}Hg were identified, while radon isotopes were observed in the ^{40}Ar + ^{166}Er and ^{48}Ca + ^{242}Pu systems.

The extracted α energies are consistent with reported values within experimental resolution, supporting the isotope assignments and decay-chain reconstruction. In addition, two-dimensional heatmaps derived from position-sensitive detector data provide spatial distributions of detected events, complementing the energy analysis.

I. Introduction

Heavy and superheavy nuclei provide a testing ground for nuclear structure at extreme proton and neutron numbers, where shell effects and stability limits are strongly modified. In particular, neutron-rich nuclei near closed shells are sensitive to changes in nuclear interactions and shell evolution.

Experimental access to this region remains limited due to low production cross sections and short half-lives. Multinucleon transfer reactions offer a practical route, as they populate a broad distribution of neutron-rich isotopes within a single experiment, enabling systematic spectroscopic studies.

Identification of these nuclei relies primarily on α-decay spectroscopy. The measured α energies, together with correlated decay sequences, provide a direct basis for isotope assignment.

At facilities such as the Flerov Laboratory of Nuclear Reactions (FLNR), setups like the MASHA mass separator combine ion extraction, mass separation, and decay detection within a single system, enabling studies of short-lived nuclei produced in heavy-ion reactions [1].

In this work, α spectra from multinucleon transfer reactions are analyzed to identify isotopes and examine their decay behaviour.

II. Theoretical Background

The structure and stability of heavy nuclei are strongly influenced by shell effects, particularly in regions close to closed neutron shells such as $N = 126$. In these systems, small changes in neutron number can significantly affect binding energies and decay properties.

For most heavy and neutron-rich nuclei, α decay is the dominant decay mode and serves as the primary observable for identification. The energy released in the decay is given by the Q-value,

$$Q_\alpha = (M_{\text{parent}} - M_{\text{daughter}} - M_\alpha)\, c^2 \tag{1}$$

where M_{parent} is the mass of the parent nucleus, M_{daughter} is the mass of the daughter nucleus, M_α is the mass of the alpha particle, and c is the speed of light. The quantity Q_α represents the total decay energy released in the alpha decay. Most of this energy is carried by the emitted alpha particle, while a small fraction appears as recoil energy of the daughter nucleus.

The decay process proceeds via quantum tunneling through the Coulomb barrier, resulting in a strong dependence of decay probability on the α energy. Consequently, measured α energies provide a direct and sensitive probe of nuclear structure.

In experimental spectra, α decays appear as discrete peaks corresponding to specific transitions. The extracted peak energies are compared with evaluated nuclear data to assign isotopes. Decay chains are then constructed by correlating successive α emissions.

In some cases, multiple peaks associated with a single isotope arise from decays to excited

states of the daughter nucleus, leading to slightly reduced α energies. These features must be accounted for during identification.

Experimental observations of increased stability with neutron number in heavy systems are consistent with shell effects and have been reported in studies of superheavy nuclei [2]. Complementary chemical investigations, such as those on element 112, further support the identification of heavy nuclei through decay properties [3].

III. Experimental Setup

The data analyzed in this work correspond to multinucleon transfer reactions ^{40}Ar + ^{148}Sm, ^{40}Ar + ^{166}Er, and ^{48}Ca + ^{242}Pu. These reactions populate a broad distribution of neutron-rich nuclei, which are subsequently separated and identified using the MASHA (Mass Analyzer of Super Heavy Atoms) setup.

The MASHA separator operates based on the ISOL technique, where reaction products are stopped, extracted, ionized, and transported through electromagnetic fields for mass-to-charge separation [4]. The overall efficiency of extraction, ionization, and transport is a critical factor in accessing nuclei with very low production cross sections [5].

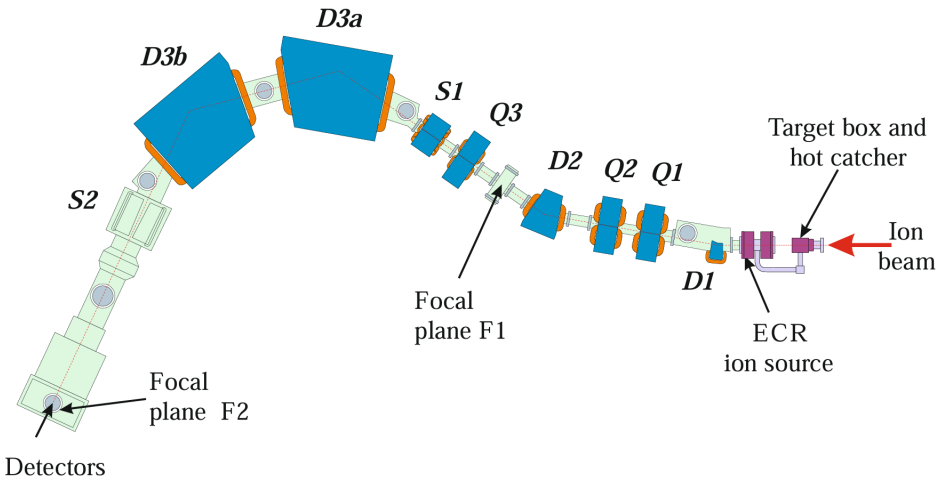

Figure 1: Scheme of the MASHA setup.

III.A. Beam and Target

Heavy-ion beams are incident on thin targets, inducing multinucleon transfer reactions and producing a wide range of neutron-rich fragments. The target assembly consists of a rotating wheel, which ensures uniform irradiation and prevents local overheating under continuous beam exposure.

Figure 2: Rotating target cassette in assembly, used for uniform irradiation of the target material.

Reaction products emerging from the target are stopped in a hot catcher positioned immediately downstream. The elevated temperature of the catcher enables rapid release of the produced nuclei, which are then extracted and directed towards the ion source.

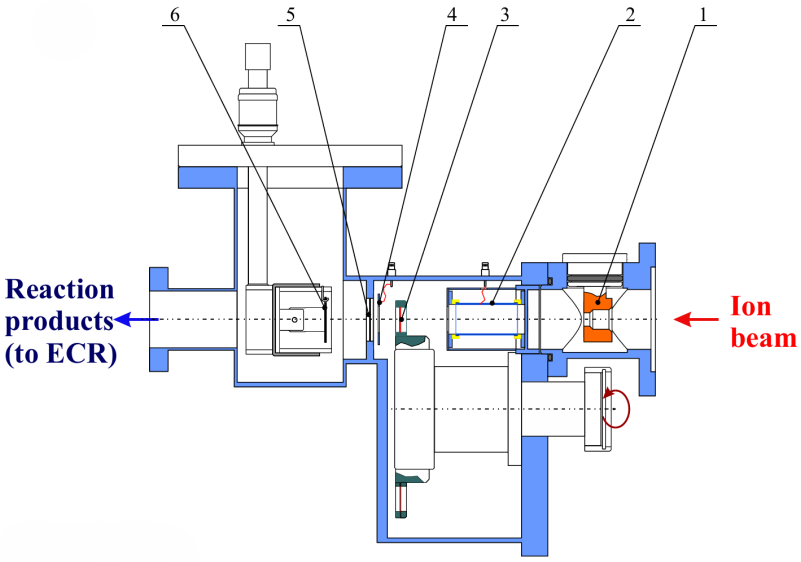

Figure 3: Schematic view of the target-hot catcher system. Here: 1– diaphragm; 2– pick-up sensor; 3– target on the wheel; 4– electron emission beam monitor; 5– separating foil; 6– hot catcher.

The extracted atoms are ionized and injected into the separator, where they are selected according to their mass-to-charge ratio.

III.B. Detector Systems

Separated nuclei are implanted into silicon strip detectors located at the focal plane. These detectors measure the energies of emitted α particles with high resolution.

The segmentation of the detectors allows simultaneous measurement of energy and position, enabling event localization and the construction of two-dimensional distributions. Each event is recorded as a pulse proportional to the deposited energy and initially digitized into detector channels, which are subsequently calibrated to obtain the corresponding α energies.

Placement at the final focal plane ensures that only mass-separated nuclei are detected, reducing background and enabling reliable identification of isotopes through their decay signatures.

IV. Methodology

The experimental data were provided as one-dimensional histograms of counts as a function of energy (keV). These spectra were analyzed to extract α-decay energies and identify the corresponding nuclei.

Peaks in the spectra were fitted using Gaussian functions to determine centroid positions. These centroid values correspond to the α-decay energies and were used for isotope identification through comparison with evaluated data. The uncertainty in peak positions arises primarily from detector resolution and fitting errors, and is estimated to be on the order of a few tens of keV.

In addition to one-dimensional spectra, two-dimensional distributions were analyzed using matrix data. These heatmaps represent counts as a function of detector strip number and energy, providing spatial information on detected events.

Energy calibration for the two-dimensional data was performed using known α energies, establishing a linear relation between detector channel number and energy. This calibration enables direct comparison between the measured spectra and reference data.

V. Data Analysis

The experimental data for all reactions were provided as one-dimensional histograms of counts as a function of alpha-particle energy. The spectra were analyzed to extract characteristic α-decay energies and identify the corresponding nuclei.

Peak centroids were determined using Gaussian fitting and compared with evaluated α-decay energies to assign transitions and construct decay chains.

The quality of Gaussian fits was evaluated using the coefficient of determination (R^2), which indicates the agreement between the fitted model and the experimental peak shapes.

In all following tables, Exp. Peak denotes the experimental peak energy, E_α the theoretical alpha-decay energy, BR(α) the alpha branching ratio, and $T_{1/2}$ the half-life.

V.A. ^{40}Ar + ^{148}Sm

The α spectra for the reaction ^{40}Ar + ^{148}Sm exhibit multiple peaks associated with mercury (Hg) isotopes and their subsequent decay products.

Prominent peaks are observed in the range $\sim$ 5500–7700 keV. The higher-energy peaks

correspond to primary α decays of Hg isotopes, while lower-energy peaks arise from decays of daughter nuclei, primarily Pt and Os.

For ^{180}Hg, a peak near ~ 6120 keV is assigned to the decay

$$^{180}\mathrm{Hg} \rightarrow ^{176}\mathrm{Pt} + \alpha,$$

while a corresponding peak near ~ 5750 keV is associated with the subsequent decay

$$^{176}\mathrm{Pt} \rightarrow ^{172}\mathrm{Os} + \alpha.$$

The same approach was applied across the isotope chain $^{181-185}$Hg, where peak positions were matched with evaluated data to establish decay sequences. The presence of correlated peaks from parent and daughter nuclei supports the consistency of these assignments.

Additional weaker structures in the spectra are attributed to less probable decay branches and residual background contributions.

The extracted peak positions and corresponding nuclear data, including α energies, half-lives, and decay pathways, are summarized in Table 1.

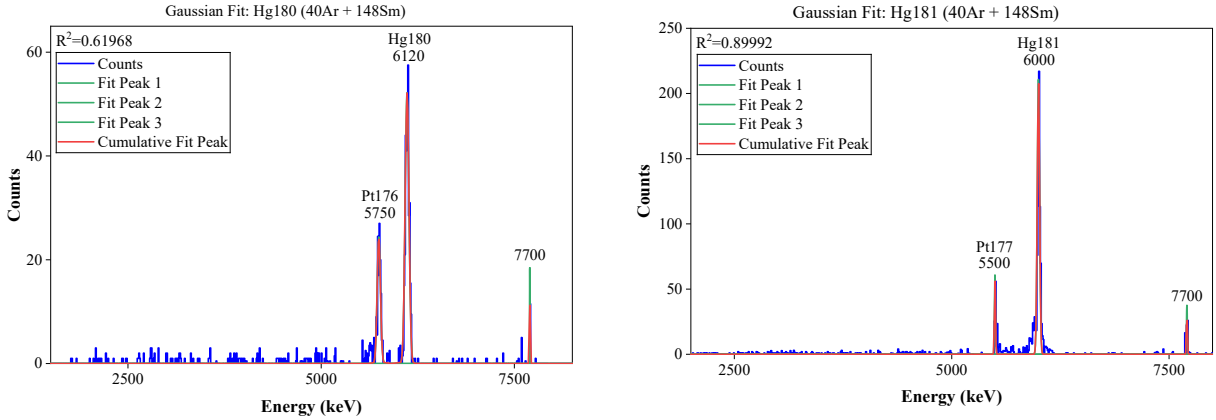

Figure 4: Alpha spectra for ^{180}Hg (left) and ^{181}Hg (right).

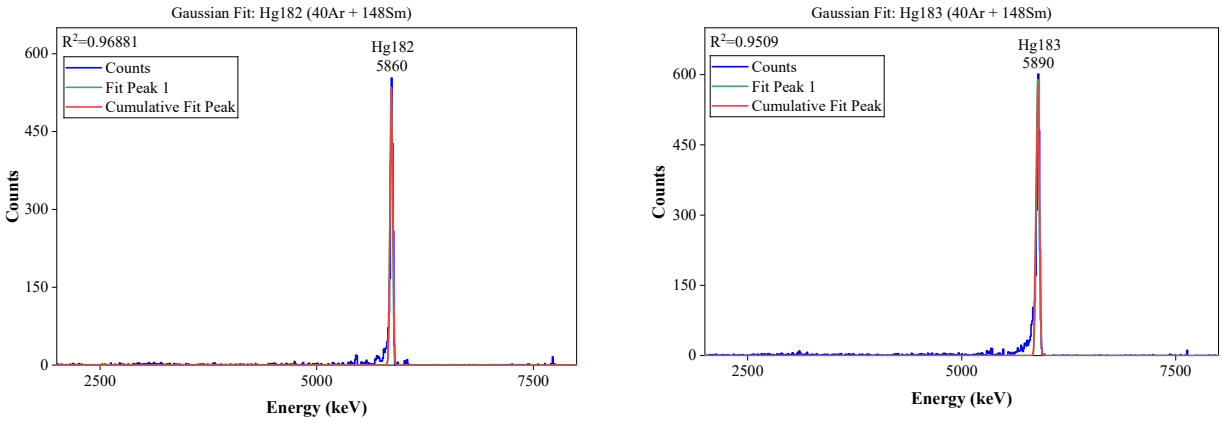

Figure 5: Alpha spectra for ^{182}Hg (left) and ^{183}Hg (right).

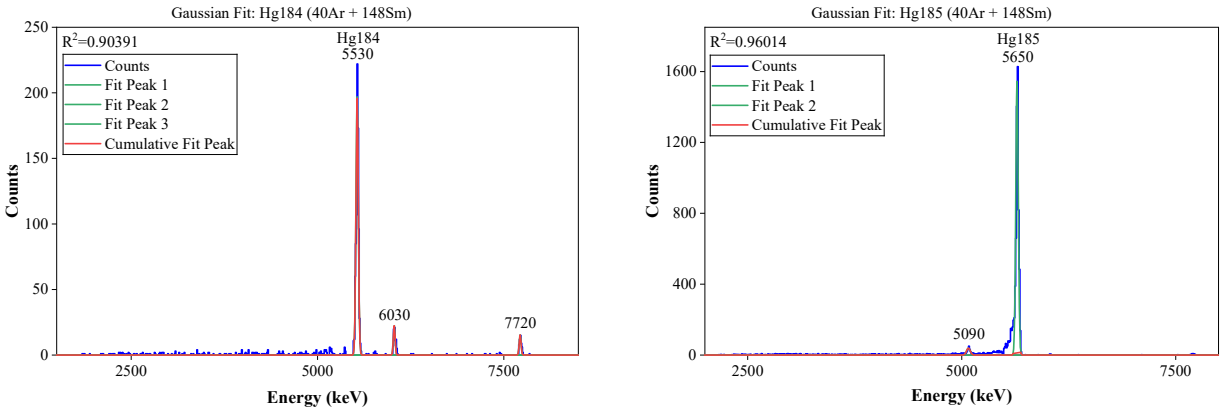

Figure 6: Alpha spectra for ^{184}Hg (left) and ^{185}Hg (right).

Parent	**Decay**	**Exp. Peak (keV)**	E_α **(keV)**	**BR** (α)	$T_{1/2}$
^{180}Hg	$^{180}\text{Hg} \rightarrow {}^{176}\text{Pt} + \alpha$	6120	6119 (99.87%)	0.48	2.58 s
	$^{176}\text{Pt} \rightarrow {}^{172}\text{Os} + \alpha$	5750	5753 (99.74%)	0.40	6.3 s
^{181}Hg	$^{181}\text{Hg} \rightarrow {}^{177}\text{Pt} + \alpha$	6000	6006 (87%)	0.3	3.54 s
	$^{177}\text{Pt} \rightarrow {}^{173}\text{Os} + \alpha$	5500	5517 (88.5%)	0.056	11 s
^{182}Hg	$^{182}\text{Hg} \rightarrow {}^{178}\text{Pt} + \alpha$	5860	5867 (99%)	0.152	10.83 s
^{183}Hg	$^{183}\text{Hg} \rightarrow {}^{179}\text{Pt} + \alpha$	5890	5904 (91%)	0.117	9.4 s
^{184}Hg	$^{184}\text{Hg} \rightarrow {}^{180}\text{Pt} + \alpha$	5530	5535 (99.44%)	0.0126	30.9 s
^{185}Hg	$^{185}\text{Hg} \rightarrow {}^{181}\text{Pt} + \alpha$	5650	5653 (96%)	0.06	49.1 s

Table 1: Identification of alpha-decay peaks and corresponding decay chains for Hg isotopes produced in the reaction ^{40}Ar + ^{148}Sm.

V.B. ^{40}Ar + ^{166}Er

The α spectra for the reaction ^{40}Ar + ^{166}Er show distinct peaks associated with radon (Rn) isotopes and their decay products.

Prominent structures are observed in the range $\sim$ 5800–6800 keV. The higher-energy peaks correspond to primary α decays of Rn isotopes, while lower-energy peaks originate from daughter nuclei, primarily Po and Pb.

For ^{201}Rn, a peak near $\sim$ 6760 keV is assigned to the decay

$$^{201}\text{Rn} \rightarrow {}^{197}\text{Po} + \alpha,$$

followed by a peak near ~ 6380 keV corresponding to

$$^{197}\text{Po} \rightarrow ^{193}\text{Pb} + \alpha.$$

This parent-daughter correlation is consistently observed across the isotope chain $^{202-205}$Rn, where peak positions align with evaluated α-decay energies. The presence of correlated transitions supports the identification of the contributing isotopes and their decay sequences.

The extracted peak positions and corresponding decay properties are summarized in Table 2.

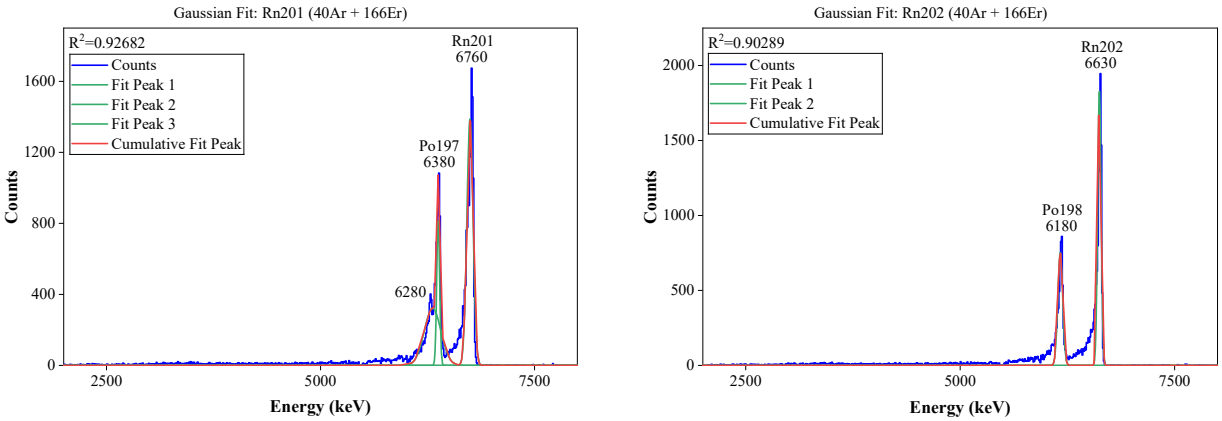

Figure 7: Alpha spectra for ^{201}Rn (left) and ^{202}Rn (right).

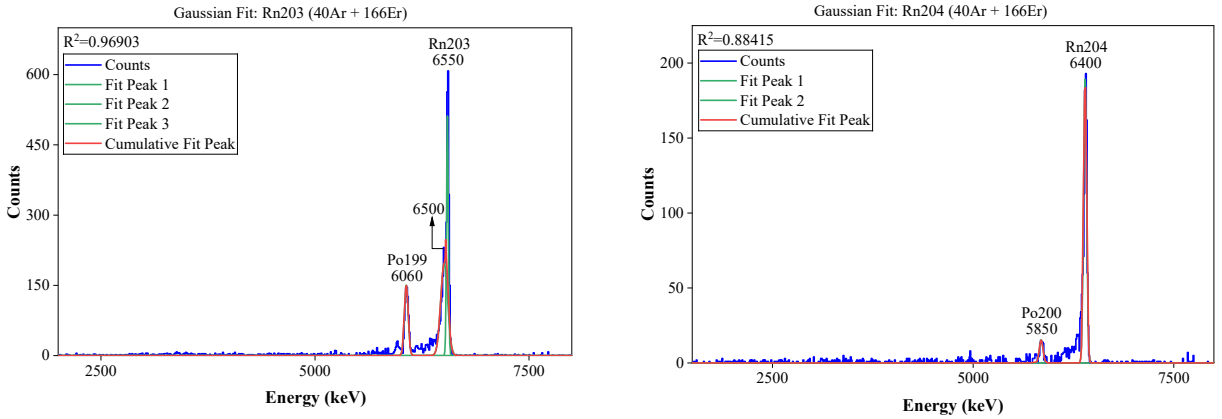

Figure 8: Alpha spectra for ^{203}Rn (left) and ^{204}Rn (right).

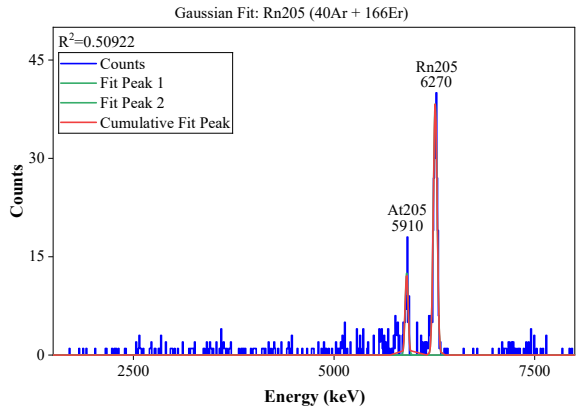

Figure 9: Alpha spectra for ^{205}Rn.

Parent	**Decay**	**Exp. Peak (keV)**	E_α **(keV)**	**BR** (α)	$T_{1/2}$
^{201}Rn	^{201}Rn $\rightarrow$ ^{197}Po + α	6760	6773 (100%)	0.90	3.8 s
	^{197}Po $\rightarrow$ ^{193}Pb + α	6380	6383.4 (99.3%)	0.84	25.8 s
^{202}Rn	^{202}Rn $\rightarrow$ ^{198}Po + α	6630	6639.5 (99.99%)	0.90	10 s
	^{198}Po $\rightarrow$ ^{194}Pb + α	6180	6182 (99.99%)	0.57	1.77 m
^{203}Rn	^{203}Rn $\rightarrow$ ^{199}Po + α	6550	6549 (100%)	0.80	28 s
	^{199}Po $\rightarrow$ ^{195}Pb + α	6060	6059 (100%)	0.39	4.17 m
^{204}Rn	^{204}Rn $\rightarrow$ ^{200}Po + α	6400	6418.9 (100%)	0.73	1.24 m
	^{200}Po $\rightarrow$ ^{196}Pb + α	5850	5861.9 (100%)	0.111	11.5 m
^{205}Rn	^{205}Rn $\rightarrow$ ^{201}Po + α	6270	6262 (98.2%)	0.23	2.83 m
	^{205}At $\rightarrow$ ^{201}Bi + α	5910	5902 (100%)	0.10	26.2 m

Table 2: Identification of alpha-decay peaks and corresponding decay chains for Rn isotopes from the reaction: ^{40}Ar + ^{166}Er.

V.C. ^{48}Ca + ^{242}Pu

The α spectra for the reaction ^{48}Ca + ^{242}Pu exhibit a more complex structure, reflecting contributions from multiple decay chains and transitions to excited states.

Peaks are observed over a broad energy range, with dominant contributions from radon (Rn) isotopes and their daughter nuclei, including Po, Bi, and Pb.

For ^{219}Rn, several peaks are identified corresponding to both ground-state and excited-state α decays,

$$^{219}\text{Rn} \rightarrow ^{215}\text{Po} + \alpha.$$

The highest-energy peak (around $\sim$ 6790 keV) is assigned to the ground-state transition,

while lower-energy peaks (e.g., $\sim$ 6530, $\sim$ 6400 keV) arise from decays populating excited states of the daughter nucleus.

Subsequent decays in the chain are also observed, including

$$^{215}\mathrm{Po} \rightarrow^{211} \mathrm{Pb} + \alpha,$$

and

$$^{211}\mathrm{Bi} \rightarrow^{207} \mathrm{Tl} + \alpha.$$

The presence of multiple peaks for a single parent nucleus reflects the population of different nuclear energy levels. These transitions are identified through comparison with evaluated α-decay energies, with excited-state decays appearing at systematically lower energies.

All identified peaks and corresponding decay properties are summarized in Table 3.

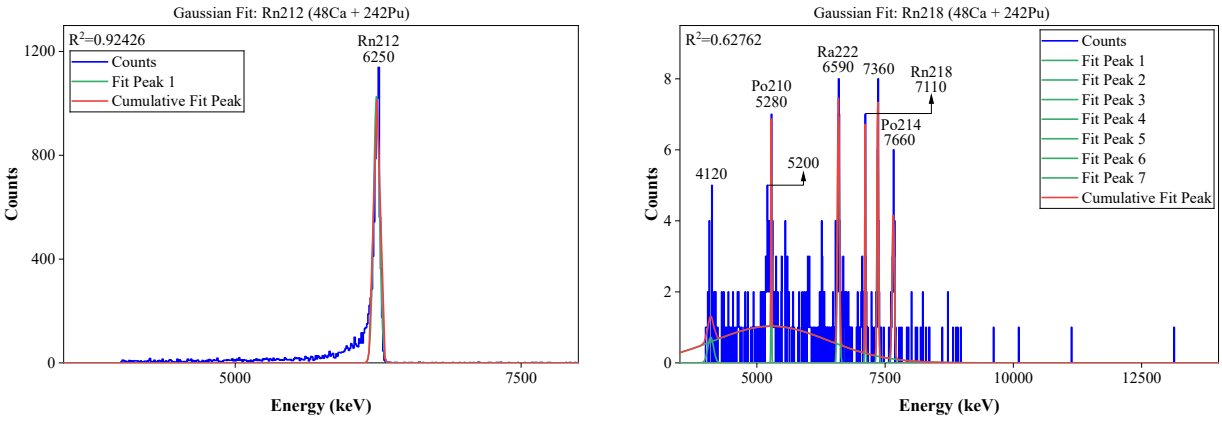

Figure 10: Alpha spectra for ^{212}Rn (left) and ^{218}Rn (right).

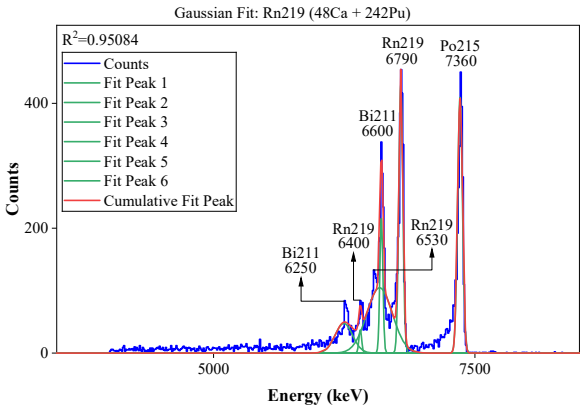

Figure 11: Alpha spectra for ^{219}Rn.

Parent	**Decay**	**Exp. Peak (keV)**	E_α **(keV)**	**BR** (α)	$T_{1/2}$
^{212}Rn	$^{212}\text{Rn} \rightarrow {}^{208}\text{Po} + \alpha$	6250	6264 (99.95%)	1.0	23.9 m
^{218}Rn	$^{222}\text{Ra} \rightarrow {}^{218}\text{Rn} + \alpha$	6590	6559 (96.9%)	1.0	36.17 s
	$^{218}\text{Rn} \rightarrow {}^{214}\text{Po} + \alpha$	7110	7129.2 (99.87%)	1.0	35 ms
	$^{214}\text{Po} \rightarrow {}^{210}\text{Pb} + \alpha$	7660	7686.82 (99.99%)	1.0	164.3 us
	$^{210}\text{Po} \rightarrow {}^{206}\text{Pb} + \alpha$	5280	5304.33 (100%)	1.0	138.376 d
^{219}Rn	$^{219}\text{Rn} \rightarrow {}^{215}\text{Po} + \alpha$	6790	6819.1 (79.4%)	1.0	3.96 s
	$^{215}\text{Po} \rightarrow {}^{211}\text{Pb} + \alpha$	7360	7386.1 (100%)	1.0	1.781 ms
	$^{211}\text{Bi} \rightarrow {}^{207}\text{Tl} + \alpha$	6600	6622.9 (83.77%)	0.997	2.14 m
	$^{219}\text{Rn} \rightarrow {}^{215}\text{Po} + \alpha$	6530	6552.6 (exc., 12.9%)	1.0	3.96 s
	$^{219}\text{Rn} \rightarrow {}^{215}\text{Po} + \alpha$	6400	6425 (exc., 7.5%)	1.0	3.96 s
	$^{211}\text{Bi} \rightarrow {}^{207}\text{Tl} + \alpha$	6250	6278.2 (exc., 16.23%)	0.997	2.14 m

Table 3: Identification of alpha-decay peaks and corresponding decay chains for Rn isotopes from the reaction: ^{48}Ca + ^{242}Pu. The notation "exc." denotes decays proceeding via excited states.

VI. Results and Discussion

The analyzed α spectra exhibit clear signatures of correlated decay chains across all studied reactions. The measured peak positions agree well with evaluated α-decay energies within experimental resolution, supporting the identification of the contributing isotopes.

For the ^{40}Ar + ^{148}Sm reaction, mercury isotopes in the range $^{180-185}$Hg are identified along with their daughter nuclei. The dominant peaks correspond to primary α decays, while additional structures arise from subsequent decays and, in some cases, transitions involving excited states.

For ^{180}Hg, the observed peak near ~ 6120 keV corresponds to the transition

$$^{180}\text{Hg} \rightarrow^{176} \text{Pt} + \alpha,$$

in agreement with the reported α energy of 6119 keV. The accompanying peak near ~ 5750 keV is associated with the decay of ^{176}Pt, confirming the presence of correlated parent-daughter sequences.

Branching ratios indicate that α decay competes with other modes such as electron capture; however, only α-decay branches contribute to the measured spectra, consistent with the detection scheme.

For the ^{48}Ca + ^{242}Pu reaction, the spectra exhibit increased complexity due to overlapping decay chains and contributions from excited states. In the case of ^{219}Rn, multiple peaks corresponding to both ground-state and excited-state transitions are resolved. The excited-state decays appear at lower energies, producing a characteristic multi-peak structure for a

single isotope.

The observation of such structures reflects the underlying level scheme of the daughter nuclei. The relative intensities of the peaks are consistent, at a qualitative level, with known branching ratios.

Overall, the consistency between measured peak positions and evaluated data supports the reliability of the identification procedure. Residual deviations can be attributed to detector resolution and uncertainties in energy calibration.

Two-dimensional heatmaps were constructed to examine the spatial distribution of detected α events as a function of detector strip and energy.

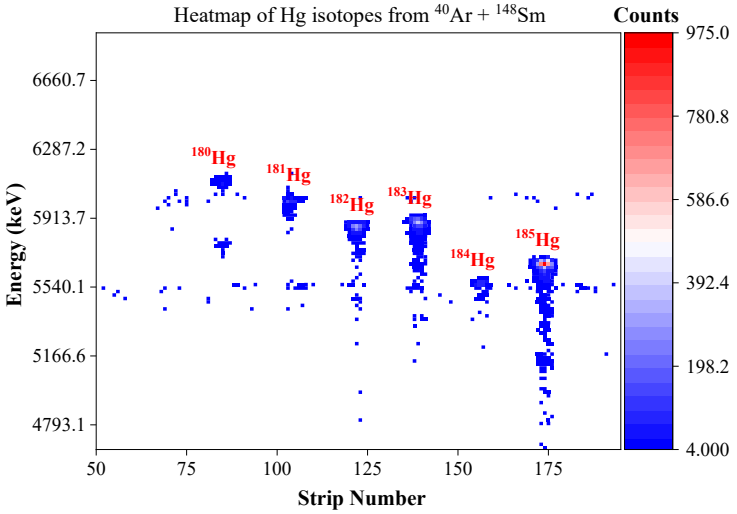

Figure 12: Heatmap of Hg isotopes from the reaction: ^{40}Ar + ^{148}Sm.

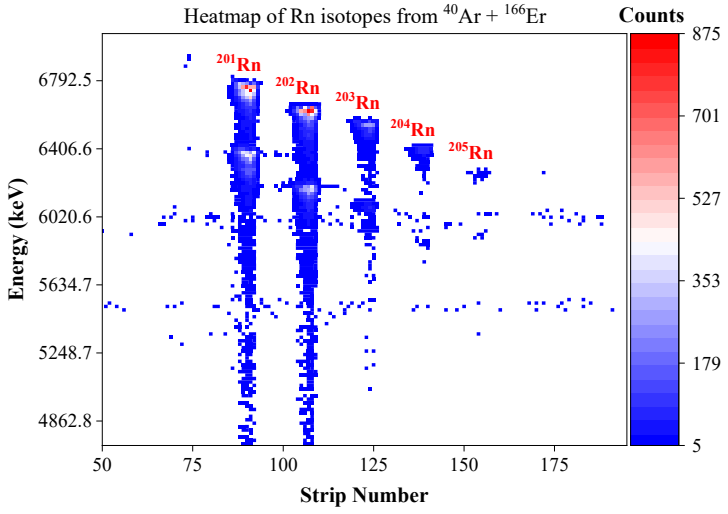

Figure 13: Heatmap of Rn isotopes from the reaction: ^{40}Ar + ^{166}Er.

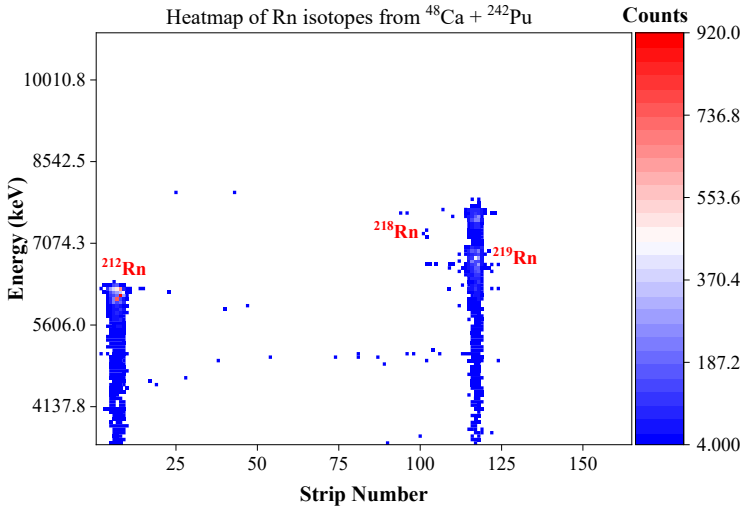

Figure 14: Heatmap of Rn isotopes from the reaction: ^{48}Ca + ^{242}Pu.

Distinct clusters are observed in the heatmaps, corresponding to individual isotopes. The alignment of these clusters along the detector strips indicates spatially resolved implantation of nuclei.

The calibrated energy axis allows direct comparison with evaluated α energies, and the positions of the clusters are consistent with those identified in the one-dimensional spectra. Similar structures are observed across all reactions, where different decay chains appear as separate bands, providing a complementary representation of the underlying decay processes.

VII. Conclusion

The analysis of α-decay spectra from multinucleon transfer reactions enabled the identification of neutron-rich nuclei through their characteristic energies and correlated decay chains.

For the ^{40}Ar + ^{148}Sm system, well-resolved peaks corresponding to Hg isotopes and their daughters were observed, while reactions involving heavier systems exhibited more complex structures arising from overlapping decay chains and contributions from excited states.

The extracted α energies are consistent with evaluated data within experimental resolution, supporting the isotope assignments and decay-chain reconstruction.

These results demonstrate that α spectroscopy, combined with mass separation, provides a consistent approach for identifying heavy nuclei and resolving their decay patterns in multinucleon transfer reactions.

Acknowledgements

I would like to thank Dr. Viacheslav Vedeneev for his guidance throughout this project. He provided the relevant literature, detailed instructions for the analysis, and the experimental datasets, along with supporting resources such as the chart of nuclides, which were essential for carrying out the work. His careful review of the report was very helpful in improving its

clarity and scientific accuracy.

I also thank the team at the Flerov Laboratory of Nuclear Reactions for providing the experimental data and for their support during the programme. Finally, I am grateful to the INTEREST programme for the opportunity to be part of this project.

References

[1] V. Y. Vedeneev, A. Rodin, L. Krupa, A. Belozerov, E. Chernysheva, S. Dmitriev, A. Gulyaev, A. Gulyaeva, D. Kamas, J. Kliman, *et al.*, Hyperfine Interactions **238**, 19 (2017).

[2] S. N. Dmitriev, Y. T. Oganessyan, V. K. Utyonkov, S. V. Shishkin, A. V. Yeremin, Y. V. Lobanov, Y. S. Tsyganov, V. I. Chepygin, E. A. Sokol, G. K. Vostokin, *et al.*, Mendeleev Communications **15**, 1 (2005).

[3] R. Eichler, N. Aksenov, A. Belozerov, G. Bozhikov, V. Chepigin, S. Dmitriev, R. Dressler, H. Gäggeler, V. Gorshkov, F. Haenssler, *et al.*, Nature **447**, 72 (2007).

[4] A. Rodin, A. Belozerov, D. Vanin, V. Y. Vedeneyev, A. Gulyaev, A. Gulyaeva, S. Dmitriev, M. Itkis, J. Kliman, N. Kondratiev, *et al.*, Instruments and Experimental Techniques **57**, 386 (2014).

[5] E. Chernysheva, A. Rodin, S. Dmitriev, A. Gulyaev, A. Komarov, A. Novoselov, Y. T. Oganessian, A. Podshibyakin, V. Salamatin, S. Stepantsov, *et al.*, in *Exotic Nuclei: Proceedings of the International Symposium on Exotic Nuclei* (World Scientific, 2020) pp. 386–390.